JOURNAL OF CATALYSIS 130, 202–211 (1991)

The Effect of Supports on the Activity and Selectivity of Co–Ni Alloy Catalysts for CO Hydrogenation

TATSUMI ISHIHARA,[1] NOBUHIKO HORIUCHI, KOICHI EGUCHI, AND HIROMICHI ARAI

Department of Materials Science and Technology, Graduate School of Engineering Sciences, Kyushu University 39, Kasuga-shi, Fukuoka 816, Japan

Received December 18, 1989; revised January 2, 1991

The CO hydrogenation activity of 50Co50Ni alloy catalysts strongly depended on the oxide support. Electron-donating oxides such as MgO, PbO, and ZnO lowered the overall activity of the 50Co50Ni metal. The CO conversion as well as the chain growth probability was high over 50Co50Ni/TiO_2 and 50Co50Ni/MnO_2. The infrared spectra of adsorbed NO indicated that the electron density of the 50Co50Ni metal was low when it was supported on electron-accepting oxide. The results of desorption measurements suggest that metal-support interaction has a great influence on the surface concentration of hydrogen and carbon monoxide, and adsorption of carbon monoxide and hydrogen is weakened by increasing the electronegativity of the oxide support. Since the rate of H_2–D_2 exchange correlated well with the CO hydrogenation rate, activation of hydrogen is of primary importance in this catalyst system. The low electron density of the alloy supported on the electron-accepting oxides such as TiO_2 and SiO_2 weakens CO adsorption, resulting in an increase in surface coverage of hydrogen. Thus sufficient coverage of hydrogen leads to a high CO hydrogenation rate.

INTRODUCTION

The primary role of a support for a metal catalyst is to provide a large surface area of an active metal for reaction. Not only the physical but also chemical effects sometimes modify the activity of metal. Vannice and Garten (*1*) have reported that the chain growth probability with Ni catalyst is enhanced when TiO_2 is used as a support as compared with Ni powder or Ni supported on SiO_2, Al_2O_3, or graphite. Santos *et al.* (*2*) have reported the charge transfer from Fe to TiO_2 with high-temperature reduction of Fe/TiO_2 ammonia synthesis catalyst. Although Vannice *et al.* have pointed out the high catalytic activity for CO hydrogenation with the use of TiO_2 support (*3, 4*), the mechanism has not been thoroughly understood. The strong metal-support interaction has been reported by Tauster *et al.* (*5*) for Group VIII noble metal on TiO_2 catalysts (*6–9*). Burch and Flambard (*10*) emphasized the creation of new active sites at the interface of Ru and TiO_2, but Raupp and Dumesic (*11*) proposed that the metals on TiO_2 support effectively serve as adsorption sites for hydrogen but not for carbon monoxide. However, only a few reports have dealt with the support effect in alloy systems (*12*).

The mixing of metal components has a great effect on the activity and the selectivity because of the electronic interaction among metals (*13*). Our previous reports (*14–17*) on the hydrogenation of CO over TiO_2-supported Fe, Co, and Ni ternary alloy catalysts have revealed that the alloy catalyst with the composition of 42Ni29Fe29Co was highly active for CO hydrogenation and the TiO_2-supported catalyst is more active for gasoline synthesis than is the SiO_2-supported one. Both the 50Co50Ni/SiO_2 and 50Co50Ni/TiO_2 systems were highly active and selective for gasoline synthesis. In this study, we have investigated the effect of the support on CO hydrogenation using the

[1] Present address: Faculty of Engineering, Oita University, Oita 870-11, Japan.

0021-9517/91 $3.00

50Co50Ni catalyst. Interaction between support oxides and the alloy particle was discussed based on results of temperature-programmed desorption (TPD) of hydrogen and carbon monoxide, infrared spectra of adsorbed NO, and the H_2–D_2 exchange reaction.

EXPERIMENTAL

Catalyst Preparation

Commercial metallic oxides, except for TiO_2, were used as supports for the 50Co50Ni catalyst. Titanium dioxide was obtained by hydrolysis of $TiCl_4$, and the precipitate was then dried and subsequently calcined at 673 K for 4 h. The supported bimetallic catalysts with total metal loading of 10 wt% were prepared by the incipient wetness technique (*14*). Calculated amounts of cobalt and nickel nitrates were dissolved in distilled water and the support oxide was soaked in the solution. Cobalt and nickel hydroxides were coprecipitated onto the support by an addition of ammonia water and the suspension was evaporated to dryness. The catalysts were calcined at 573 K for 2 h in air and 673 K for 2 h under H_2 stream. The phases of 50Co50Ni alloy and oxide supports were identified by powder X-ray diffraction just after reduction.

Apparatus and Procedure

Catalytic hydrogenation of carbon monoxide was performed in a high-pressure fixed-bed flow reactor, as reported previously (*14*). The catalyst was preheated in a hydrogen stream at 523 K for 1 h before reaction. A gaseous mixture of H_2 (62 vol%), CO (33 vol%), and Ar (5 vol%), which was freed of water and carbonyl impurities by active carbon and 13 X-type zeolite, was fed to the catalyst bed at W/F = 10 g-cat · h/mol, where W is the catalyst weight and F is the total flow rate. Unless otherwise noted, the reaction data were taken at 523 K and the total pressure was fixed at 1.0 MPa. The reaction products were analyzed by gas chromatography (*16*).

Temperature-programmed desorption of hydrogen and carbon monoxide was measured in a flow system. The apparatus and the experimental procedure were described in a previous paper (*14*). A catalyst was reduced in a hydrogen stream at 673 K for 1 h and was evacuated at room temperature for 0.5 h before the TPD measurement of H_2. Carbon monoxide was adsorbed on the prereduced catalysts at 673 K and then evacuated at room temperature. Purified argon and helium were used as carrier gases for TPD of H_2 and CO, respectively, after impurity oxygen was removed by electrochemical pumping using yttria-stabilized zirconia (YSZ) as an electrolyte. During heating in a programmed schedule (9 K/min), desorption of hydrogen or carbon monoxide from the sample was monitored by two thermal-conductivity detectors (TCD). Water and carbon dioxide were removed with a cold trap which was placed between the detectors.

In situ infrared spectra were recorded with a JASCO IR-810 spectrometer (*18*). A sample disk was heated at 673 K for 3 h *in vacuo* to remove water and other adsorbed gases. Nitrogen monoxide (ca. 4×10^3 Pa) was introduced to the sample at room temperature and heated to 423 K. After adsorption, nitrogen monoxide in the gas phase was evacuated at room temperature prior to the IR measurement. The background spectrum of the catalyst without the adsorption treatment was subtracted from the observed spectrum.

The H_2–D_2 exchange reaction was carried out in a conventional closed circulating system of 120 cm^3 volume. Gaseous deuterium was obtained by electrolysis of D_2O. Commercial hydrogen was purified by a liquid N_2 trap. The mixture, with equal amounts of H_2 and D_2 (total pressure 29.3 kPa), was circulated and the isotopes were analyzed by gas chromatography using a $MnCl_2$/Al_2O_3 (10 wt%) column (*19*). Before the exchange reaction, the catalyst (0.3 g) was reduced with H_2 (ca. 100 Torr) at 673 K for 1 h and then evacuated at 673 K for 1 h. The

TABLE 1

Lattice Constant and Average Particle Size of Co–Ni Alloy Catalysts

Support	S.A.[a] ($m^2\ g^{-1}$)	Lattice constant (nm)	Particle size[b] (nm)
MgO	96.3	0.3531	16.6
PbO	1.5	0.3530	19.8
ZnO	10.5	0.3526	11.7
Al_2O_3	200.7	0.3527	10.1
Cr_2O_3	1.5	0.3528	20.7
TiO_2	43.0	0.3526	17.5
MnO_2	25.4	0.3530	15.6
V_2O_5	7.7	0.3529	12.7
Nb_2O_5	8.0	0.3527	17.2
ZrO_2	10.8	0.3528	11.9
SiO_2	380.0	0.3529	16.1
MoO_3	19.8	0.3528	15.2
Pentasil	320.0	0.3530	16.5

Note. Lattice constants of Co and Ni are 0.3520 nm and 0.3540 nm, respectively.

[a] Surface area of support.

[b] Average particle size.

rate of H_2–D_2 exchange, r, was obtained from

$$\log(X_0 - X_e)/(X_t - X_e) = rt/2.303N,$$

where t and N are the reaction time and the total molar amount of hydrogen (H_2 + D_2 + HD) in the system, respectively, and X_0, X_t, and X_e are the molar fractions of HD at 0 s, t s, and equilibrium state, respectively (*20, 21*).

RESULTS

Phases and Particle Sizes of Alloy

The phases and lattice constants of the catalysts were observed by X-ray diffraction after reduction at 673 K. Only the strongest diffraction peak from 50Co50Ni alloy was detected except for the peaks from the support oxide. The lattice constant of 50Co50Ni alloy estimated from this peak is given in Table 1. Since the lattice constant of the supported 50Co50Ni bimetallic catalyst was an intermediate value between those of Co and Ni, it is assumed that supported 50Co50Ni bimetal formed the fcc structured alloy on the support oxide (*21*). An average particle size of the supported metal was obtained from the Scherrer equation by line broadening analysis (Table 1). The average particle size of 50Co50Ni alloy ranging from 10 to 20 nm depends on the kind of support oxide.

Infrared Spectra of Adsorbed NO

Infrared spectra of adsorbed CO has often been employed for CO hydrogenation catalysts; however, the amount of molecular adsorbed CO is small on this 50Co50Ni alloy because of its high dissociation activity. We have previously reported on the electronic state of Fe–Co, Co–Ni, and Ni–Fe bimetallic systems as deduced from IR investigation of adsorbed NO (*18*). The infrared spectra of adsorbed NO are sensitive enough to study the electronic state of metals (*22, 23*). Figure 1 shows the infrared spectra of adsorbed NO on 50Co50Ni supported on MgO, Al_2O_3, ZrO_2, SiO_2, and H-pentasil-type zeolite. Two infrared bands around 1800 and 1860 cm^{-1} generally appeared, ex-

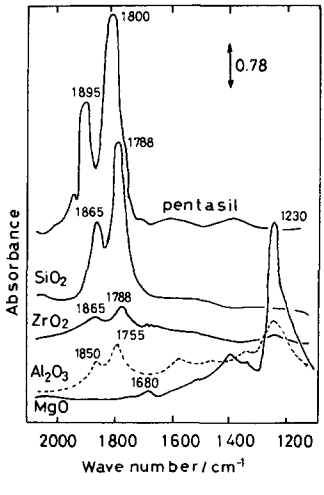

FIG. 1. Infrared spectra of adsorbed NO over supported 50Co50Ni alloy catalysts.

TABLE 2

Hydrogenation of Carbon Monoxide over Co–Ni Alloy Catalyst Supported on Various Oxides

Support	CO conv. (%)	Selectivity (%)[a]					
		CH_4	$C_2^=-C_4^=$	$C_2^--C_4^-$	C_5-C_{11}	C_{12+}	Oxy.
MgO	0.1	100	0	0	0	0	0
PbO	0.1	100	0	0	0	0	0
ZnO	0.1	25.7	7.2	7.5	0	0	59.6
Al_2O_3	18.8	27.3	10.5	19.4	39.6	3.3	0.1
Cr_2O_3	34.0	24.6	2.9	28.8	40.3	2.2	1.2
TiO_2	46.0	15.0	17.3	22.1	44.0	1.0	6.0
MnO_2	24.2	19.5	7.9	30.1	40.5	1.8	0.1
V_2O_5	9.5	11.9	21.7	16.8	41.6	5.8	2.2
Nb_2O_5	14.7	21.4	10.8	24.7	40.5	0	0.1
ZrO_2	13.2	36.5	4.7	24.2	28.8	4.7	0.1
SiO_2	32.3	33.4	1.8	28.7	35.5	0.5	0
MoO_3	2.2	35.9	24.2	27.4	11.4	0	1.2
Pentasil	32.8	45.8	3.4	27.6	23.2	0	0

[a] Calculation based on carbon number: 523 K, 1.0 MPa, $H_2/CO = 2.0$, $W/F = 10$ g-cat · h/mol. $C_2^=-C_4^=$, olefins; $C_2^--C_4^-$, paraffins; C_5-C_{11}, gasoline fraction; C_{12+}, higher hydrocarbons than carbon number of 11; oxy., oxygenated compounds such as alcohols, ketones.

cept for 50Co50Ni/MgO. Absorption bands below 1700 cm^{-1} on 50Co50Ni/MgO and 50Co50Ni/Al_2O_3 are assigned to the NO species adsorbed on the support oxides because they are also observable on pure MgO and Al_2O_3. The absorption bands around 1800 and 1860 cm^{-1} can be assigned to bent- and linear-type NO, respectively, based on our previous work (*18*). The bent- and linear-type NO was absent on 50Co50Ni/MgO, but these band intensities were very strong on zeolite- and SiO_2-supported catalysts. The intensity of bent-type NO is related with the number of active sites for the CO hydrogenation, as reported in our previous study (*18*). The strong bent-type NO band on SiO_2- and zeolite-supported catalysts suggests that there are numerous adsorption sites on these catalysts. The absorption band of NO shifted to slightly higher frequency in the case of electron-accepting oxides such as SiO_2. This shift is likely to be due to the low electron density of the alloy.

Hydrogenation of Carbon Monoxide

The activity and the product distribution over the 50Co50Ni catalyst on various oxides are summarized in Table 2, where the product distribution is expressed with reference to a CO base. Carbon dioxide was scarcely formed over all the supported 50Co50Ni catalysts. The catalytic activity as well as the product distribution are strongly influenced by the kind of oxide support. A high dispersion of metal does not always result in high CO conversion, as shown in Table 2. The main factor, which determines the catalytic activity, appears to be chemical interaction between the support and the metal. Support oxides such as MgO, ZnO, and PbO lowered the overall activity of the 50Co50Ni catalyst, but the activity as well as the chain growth probability was enhanced by using the oxide supports Cr_2O_3, TiO_2, and MnO_2. Among the catalysts in Table 2, the overall yield of the gasoline fraction (C_5-C_{11}) was highest on the TiO_2-supported catalyst. Silica and pentasil-type zeolite were also effective in enhancing CO conversion; however, methanation proceeded preferentially to the chain growth reaction. The vanadia-supported catalyst exhibited the highest chain growth probability as well as a high selectivity to olefins. The catalyst supported on MoO_3 was also selective for the production of C_2-C_4 olefins.

Adsorption States of Hydrogen and Carbon Monoxide

Temperature-programmed desorption is powerful in determining the adsorption state of H_2 and CO (*24–26*). Hydrogen and carbon monoxide desorption in TPD strongly depends on the support oxides, as shown in Figs. 2 and 3. A large amount of hydrogen desorption was observed from 50Co50Ni/V_2O_5 and 50Co50Ni/MoO_3 catalysts, as a result of spillover (*27, 28*). The amount of H_2 desorption below 523 K was small on MgO-, ZnO-, and Al_2O_3-supported catalysts, but large on SiO_2-, ZrO_2-, and TiO_2-supported ones (Fig. 2). As discussed later, the desorption temperature is related with the catalytic activities for CO hydrogenation.

The amount of CO desorption was gener-

ally larger than that of H_2. Most of CO on the catalysts desorbed above 673 K, as shown in Fig. 3. This suggests that adsorption of CO is strong compared with that of H_2. The large amount of CO_2 desorption observed on MgO- and Al_2O_3-supported catalysts was formed by disproportionation of adsorbed CO.

H_2–D_2 Exchange Reaction

The rates of the H_2–D_2 exchange reaction on the 50Co50Ni alloy catalysts are summarized in Table 3. The exchange rate on 50Co50Ni/MgO was extremely fast, and HD formed even at 77 K. The high activity of 50Co50Ni/MgO suggests that HD formed not only on the Co–Ni alloy but also on the MgO surface (*29*). The exchange rates on Co–Ni alloy catalysts except for Co–Ni/MgO were at a similar level, but no relation has been found between the CO hydrogenation activity and H_2–D_2 exchange rate. Preadsorbed carbon monoxide greatly lowered the overall rate of H_2–D_2 exchange. The formation of HD did not proceed on 50Co50Ni/MgO at 298 K. This suggests that the adsorption of CO is much stronger than that of hydrogen (*30*). The H_2–D_2 exchange reaction is strongly impeded by preadsorbed CO on the electron-donating oxides because of their strong affinity for CO.

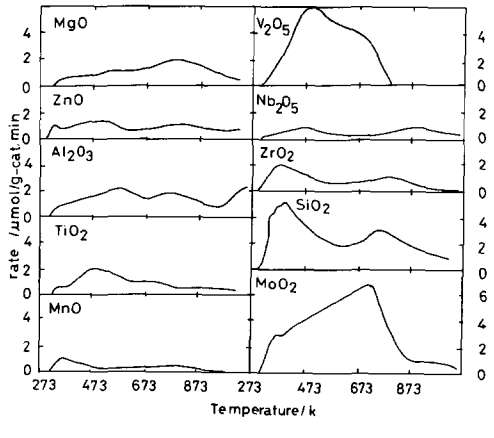

FIG. 2. TPD curves of H_2 from supported 50Co50Ni catalysts.

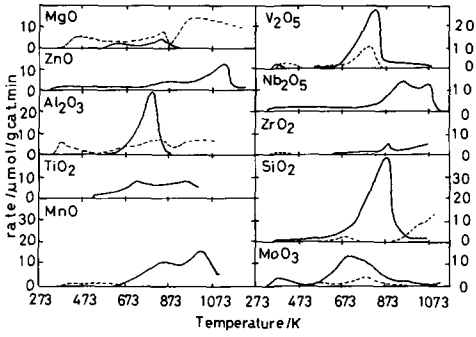

FIG. 3. TPD curves of CO from supported 50Co50Ni catalysts. (—) CO; (---) CO_2.

DISCUSSION

Phases and Particle Size of Alloy

The diffraction peak from the (111) plane of Co–Ni alloy is always detected on the supported 50Co50Ni catalysts. The lattice constant of the alloy is unchanged by the support. It is reported that the surface of Co–Ni alloy is enriched with cobalt (*21*). The absorbance of bent- and linear-type NO seems to reflect the number of electron-donating and electron-withdrawal sites, respectively. The ratio of absorbance of bent- to linear-type NO, therefore, qualitatively reflects the electron-donating property of the surface adsorption sites of Co–Ni alloy. It is expected that the electronic state of adsorption sites on alloy would alter linearly from Co to Ni as a result of the electronic interaction between Co and Ni, which is suggested by XPS measurements (*31*). The ratio of these two NO absorption bands, therefore, linearly decreased with increasing Ni content in the bulk alloy. Thus the ratio of the absorbance of bent- to linear-type NO seems to reflect the surface composition of Co–Ni alloy. Two infrared bands assigned to bent- and linear-type NO always appeared on supported Co–Ni catalyst except for 50Co50Ni/MgO (Fig. 1). The surface composition of Co–Ni is almost similar on every supported 50Co50Ni catalyst in Fig. 1 judging from the ratio of the absorbance of bent- to linear-type NO.

TABLE 3

Rates of H_2–D_2 Exchange Reaction over Supported Co–Ni Alloy Catalysts

Support	Before CO adsorption				After CO adsorption		
	H_2–D_2 Exchange rate (mol/min)			E^a (kcal/mol)	H_2–D_2 Exchange rate (mol/min)		E^a (kcal/mol)
	77 K	195 K	273 K		195 K	273 K	
MgO	5.93×10^{-5}	3.31×10^{-3}	[b]	1.1	[c]	[c]	—
Al_2O_3	[c]	1.15×10^{-4}	2.65×10^{-3}	4.2	6.28×10^{-6}	2.65×10^{-5}	9.3
V_2O_5	[c]	9.71×10^{-5}	2.61×10^{-3}	4.4	7.07×10^{-6}	1.85×10^{-5}	6.2
TiO_2	[c]	3.04×10^{-5}	1.27×10^{-3}	5.0	3.80×10^{-6}	3.16×10^{-5}	13.7
SiO_2	[c]	3.89×10^{-4}	1.63×10^{-3}	1.7	1.69×10^{-5}	8.45×10^{-5}	6.9

[a] Activation energy.
[b] Exchange rate $>1 \times 10^{-2}$ mol/min.
[c] Exchange rate $<1 \times 10^{-6}$ mol/min.

The remarkable support effects on the catalytic activity should partly result from the particle size of the metal. However, a high dispersion of metal does not always result in a high CO conversion, as shown in Tables 1 and 2. The variation in the activity and the selectivity of supported 50Co50Ni catalysts is expected to be more strongly influenced by a chemical interaction between the support and 50Co50Ni alloy.

Electronic Interaction between Alloy and Support Oxide

The bent-type (NO^-) is formed by electron donation from the metal to the antibonding orbital of the NO molecule, whereas linear-type (NO^+) is formed by electron withdrawal from NO. With an electron donation from metal to NO, both bent- and linear-type bands shifted to lower frequencies (*18, 32*). The absorption frequency of NO depends on the support oxide (Fig. 1). This suggests that support oxide interacts electronically with Co–Ni alloy. The electron-accepting property of the oxide can be expressed by the electronegativity scale. The geometric mean of the electronegativities of components is defined as the electronegativity of oxide based on the Sanderson rule (*33*). The absorption frequency of bent-type NO is shown in Fig. 4 as a function of the electronegativity of the support oxide. The absorption frequency of bent-type NO is shifted to higher frequencies on increasing the electronegativity of support oxide. The support effects proposed up to now are electronic interaction between metal and support (*34–36*), morphological effects such as the ensemble effect, alloy formation with support, and migration of partially reduced support to the metal surface. The electron transfer model was supported by the infrared shifts of the NO bands depending on the electron-accepting property of the oxide (Fig. 4). Theoretical calculation, however, suggests that electronic perturbations in the

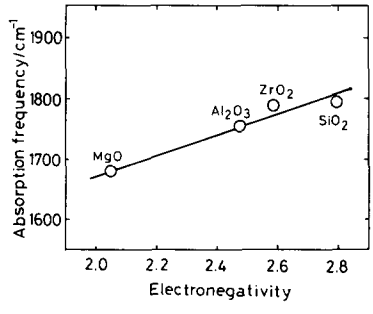

FIG. 4. Relation between electronegativity of oxides and the absorption frequency of bent-type NO.

present metal particles is small because of their large size (*37*). The effect of the support oxide cannot be explained by the pure electron-transfer model. Burch and Flambard (*10*) and Zhao and Chung (*38*) proposed that the active sites at the metal and oxide support interface play the decisive role for the CO hydrogenation. In the present Co–Ni alloy catalyst, these perimeter sites are also expected to play an important role for the CO hydrogenation reaction. The electronic state of the perimeter sites on Co–Ni alloy seems to be strongly affected by the electronic interaction between metal and supported oxide. The number of perimeter sites depends on the average particle size of alloy. However, no relationship can be observed between the average particle size and the catalytic activity and selectivity of the alloy. Since the average particle size of the alloy is distributed in a rather narrow range from 10 to 20 nm, as shown in Table 1, the difference in the electronic state of perimeter sites seems to affect strongly the adsorption and catalytic properties of the alloy as compared with the difference in the number of perimeter sites.

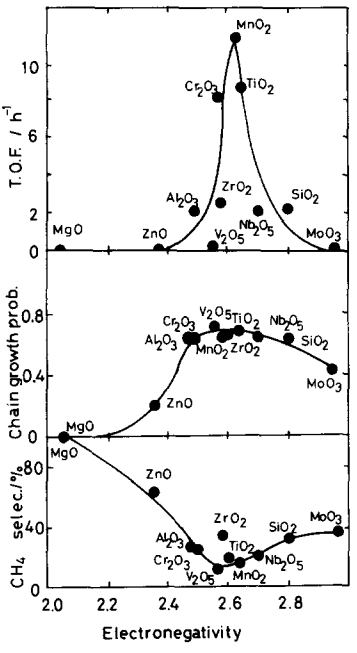

FIG. 5. Relation between electronegativity of oxides and turnover frequency (TOF), chain growth probability, and CH_4 selectivity.

Relation between the Electronegativity of Support Oxides and CO Hydrogenation

The turnover frequency for CO hydrogenation, chain growth probability, and the methane selectivity are plotted as a function of the electronegativity of the support oxides in Fig. 5. The turnover frequency for CO hydrogenation was calculated based on the amount of adsorbed hydrogen. An exceptionally large amount of hydrogen due to spillover desorbs from V_2O_5- and MoO_3-supported Co–Ni alloy. It is noted, therefore, that the turnover frequencies of V_2O_5- and MoO_3-supported Co–Ni alloy catalysts were estimated as rather small values. As the electronegativity of the support increases, the turnover frequency increases until it reaches a maximum around the electronegativity of 2.6. The chain growth probability was also maximum at an intermediate electronegativity. The dependence of CH_4 selectivity on electronegativity is almost reverse to that of the chain growth probability. Although the influence of the difference in the number of perimeter sites is small as compared with the electronic effects, the deviation in the correlation in Fig. 5 seems to be brought about by the particle size effect. The effect of electronegativity is further investigated in connection with adsorption behavior for carbon monoxide and hydrogen.

Relation between the CO Hydrogenation and the Adsorption Property of Co–Ni Alloy

The temperatures at the maximum rates of H_2 (Fig. 2) and CO desorption (Fig. 3) in the TPD experiments are plotted as a function of electronegativity of the support oxide in Fig. 6. Both H_2 and CO desorbed in a relatively low-temperature region from 50Co50Ni metal on oxides with high electronegativity. The electron density of adsorp-

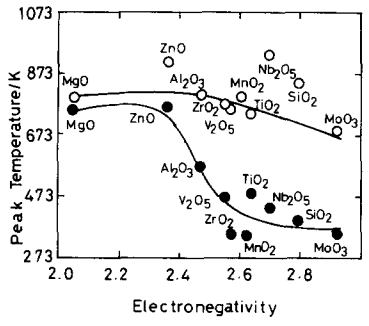

FIG. 6. Dependence of the desorption temperature of H_2 and CO on the electronegativity of oxide support. ● H_2 desorption; ○ CO desorption.

tion sites is lowered by electron withdrawal from the electron-accepting oxide. The chemical bonds between the metal and hydrogen or carbon monoxide should be weakened. A large amount of CO_2 desorbed from the catalysts on the electron-donating oxides such as MgO or Al_2O_3, but only a small amount from those on electron-accepting oxides such as SiO_2 or Nb_2O_5 (Fig. 3). The low electron density of adsorption sites suppresses the dissociative chemisorption of CO. Thus the electron density of adsorption sites has a great influence on the adsorption property of the alloy.

The H_2–D_2 exchange reaction was strongly suppressed by CO adsorption (Table 3). No relation has been found between the activities for CO hydrogenation and H_2–D_2 exchange reaction without CO adsorption. The amount of adsorbed hydrogen and carbon monoxide almost corresponds to that estimated from the average particle size in Table 1. However, the amount of adsorbed carbon monoxide is generally larger than that of hydrogen. In addition, the desorption temperature of carbon monoxide is higher than that of hydrogen (Fig. 6). It is expected that the adsorption of carbon monoxide is faster and stronger than that of hydrogen. As with other metal catalyst systems, adsorption of hydrogen is strongly impeded by CO adsorption (*39–41*). The overall rate for CO hydrogenation is then plotted versus the rate of H_2–D_2 exchange at 523 K on CO preadsorbed 50Co50Ni alloy. The exchange rate is estimated by extrapolation of the Arrhenius plots in Fig. 7. The CO hydrogenation rate evidently correlates well with the H_2–D_2 exchange rate at 523 K. The hydrogen activation ability in the presence of CO is of primary importance in determining the catalytic activity of the Co–Ni catalysts.

The TPD experiments in Fig. 2 revealed the existence of two hydrogen species on alloy catalysts, viz., hydrogen desorbed below 473 K and above 673 K. Weakly bonded hydrogen is generally regarded as active for the hydrogenation reaction in other systems (*42, 43*). We have reported previously (*16*) that, in a series of Fe–Co–Ni catalysts supported on TiO_2 or SiO_2, the amount of hydrogen desorbed at 423–473 K correlates with the CO conversion. The CO conversion of supported 50Co50Ni catalysts is plotted as a function of the amount of hydrogen desorbed at 423–473 K in Fig. 8. The 50Co50Ni/V_2O_5 and 50Co50Ni/MoO_3 catalysts are excluded from the plot because of exceptionally large desorption due to spill-

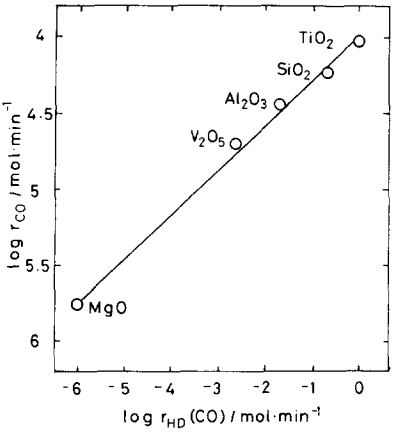

FIG. 7. Relation between the rate of CO hydrogenation, r_{CO}, and H_2–D_2 exchange rate, r_{HD}, at 523 K. H_2–D_2 exchange rate under conditions of saturated CO adsorption was carried out after preadsorption of CO and was estimated by extrapolation of the Arrhenius plots.

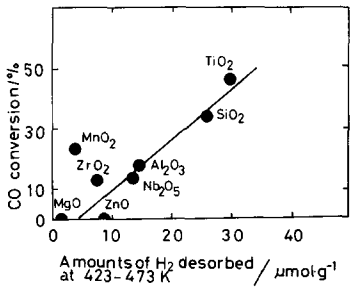

FIG. 8. Plots of CO conversion versus the amount of desorbed H_2 at 423–473 K.

over (*27, 28*). The good correlation between the CO conversion and the amount of hydrogen desorption suggests that the weakly bonded hydrogen is active for the CO hydrogenation. The high CO hydrogenation and H_2–D_2 exchange rates on TiO_2- or SiO_2-supported catalyst are attributed to the high concentration of active hydrogen on the alloy surface. Considering the TPD data in Fig. 3, the chemisorption of carbon monoxide is so strong on the basic oxides that no room exists for hydrogen adsorption on the metal surface. On the contrary, hydrogen adsorption proceeded rapidly on the metal supported on the electron-accepting oxides. Thus, methanation proceeded dominantly on the alloy supported on SiO_2 or zeolite. High chain growth probability was obtained on the 50Co50Ni alloy supported on Cr_2O_3, TiO_2, or V_2O_5 because both hydrogen and carbon monoxide are easily chemisorbed and form the intermediate of partially hydrogenated species on the catalyst surface.

The migration of partially reduced support species to the metallic surface may occur on some catalysts, such as the TiO_2-supported one. However, it can be recognized that there is a significant support effect among the Co–Ni alloys supported on the non-reducible oxides such as Al_2O_3, SiO_2, and MgO. Considering the infrared shifts of the NO bands, electronic interaction at the metal-oxide interface gives a very significant effect as compared with the migration of partially reduced support species to the metallic surface in the Co–Ni alloy system.

CONCLUSION

The oxide support exhibits marked effects on both the CO hydrogenation activity and the product distribution of the 50Co50Ni alloy. The adsorption and activation of hydrogen is of primary importance in determining the catalytic activity of the system, since the surface CO species strongly hinder hydrogen adsorption. Support oxides such as Cr_2O_3, TiO_2, or V_2O_5 are most effective in producing a gasoline fraction. The support effect in the present study seems to result from control of the surface concentrations of active hydrogen.

REFERENCES

1. Vannice, M. A., and Garten, R. L., *J. Catal.* **56,** 236 (1979).
2. Santos, J., Phillips, J., and Dumesic, J. A., *J. Catal.* **81,** 147 (1980).
3. Vannice, M. A., and Garten, R. L., *J. Catal.* **63,** 255 (1980).
4. Smith, J. S., Thrower, P. A., and Vannice, M. A., *J. Catal.* **68,** 270 (1981).
5. Tauster, S. J., Fung, S. C., and Garten, R. L., *J. Am. Chem. Soc.* **100,** 170 (1978).
6. Sadeghi, H. R., and Henrich, V. E., *J. Catal.* **87,** 279 (1984).
7. Singh, A. K., Pande, N. K., and Bell, A. T., *J. Catal.* **94,** 442 (1985).
8. Marcelin, G., Ko, E. I., and Lester, J. E., *J. Catal.* **96,** 202 (1985).
9. Belton, D. N., Sun, Y. M., and White, J. M., *J. Phys. Chem.* **88,** 5172 (1984).
10. Burch, R., and Flambard, A. R., *J. Catal.* **78,** 389 (1982).
11. Raupp, G. B., and Dumesic, J. A., *J. Catal.* **95,** 587 (1985).
12. Jiang, X. Z., Stevenson, S. T., and Dumesic, J., *J. Catal.* **91,** 11 (1985).
13. Burch, R., *Acc. Chem. Res.*, 24 (1982).
14. Arai, H., Mitsuishi, K., and Seiyama, T., *Chem. Lett.*, 1291 (1984).
15. Ishihara, T., Eguchi, K., and Arai, H., *Appl. Catal.* **30,** 225 (1987).
16. Ishihara, T., Eguchi, K., and Arai, H., *Appl. Catal.* **40,** 87 (1988).
17. Horiuchi, N., Ishihara, T., Eguchi, K., and Arai, H., *Chem. Lett.*, 499 (1988).
18. Ishihara, T., Eguchi, K., and Arai, H., *Chem. Lett.*, 1695 (1986).
19. West, D. L., and Marson, A. L., *J. Am. Chem. Soc.* **80,** 4731 (1964).
20. Ohno, S., and Yasumori, I., *Bull. Chem. Soc. Jpn.* **41,** 2227 (1968).

21. Matsuyama, M., Ashida, K., Takayasu, O., and Takeuchi, T., *J. Catal.* **102,** 309 (1986).
22. Arai, H., and Tominaga, H., *J. Catal.* **43,** 131 (1976).
23. Niiyama, H., and Echigoya, E., *J. Catal.* **38,** 238 (1975).
24. Gorte, R. J., *J. Catal.* **75,** 164 (1982).
25. Forni, L., and Magni, E., *J. Catal.* **112,** 437 and 444 (1988).
26. Hery, R. K., Kiela, J. B., and Marin, S. P., *J. Catal.* **73,** 66 (1982).
27. Sermon, P. A., and Bond, G. C., *Catal. Rev.-Sci. Eng.* **8,** 211 (1973).
28. Conner, W. C., Pajonk, G. M., and Teichner, S. J., *in* "Advances in Catalysis" (D. D. Eley, H. Pines, and P. B. Weisz, Eds.), Vol. 34, p. 1. Academic Press, San Diego, 1986.
29. Indovina, V., Cimino, A., Inversi, M., and Pepe, F., *J. Catal.* **58,** 396 (1979).
30. Tomotsu, N., Kojima, I., and Yasumori, I., *J. Catal.* **86,** 280 (1984).
31. Ishihara, T., Inoue, T., Eguchi, K., Takita, Y., Arai, H., to be published.
32. King, D. L., and Peri, J. B., *J. Catal.* **79,** 164 (1983).
33. Sanderson, R. T., "Chemical Bonds and Bond Energy." Academic press, New York, 1976.
34. Hermann, J. M., *J. Catal.* **89,** 404 (1984).
35. Bracey, J. D., and Burch, R., *J. Catal.* **86,** 384 (1984).
36. Kao, C. C., Tsai, S. C., and Chung, Y. W., *J. Catal.* **73,** 139 (1982).
37. Joyner, R. W., Pendry, J. B., Saldin, D. K., and Tennison, S. R., *Surf. Sci.* **138,** 84 (1984).
38. Zhao, Y., and Chung, Y., *J. Catal.* **106,** 369 (1987).
39. Raupp, G. P., and Dumesic, J. A., "Strong Metal-Support Interactions," p. 34. American Chemical Society, Washington DC, 1986.
40. Paal, Z., and Menon, P. G., *Catal. Rev.-Sci. Eng.* **25,** 229 (1983).
41. Breiter, M. W., *Electrochim. Acta* **29,** 711 (1984).
42. Blackmond, D. G., and Ko, E. I., *J. Catal.* **94,** 343 (1985).
43. Menon, P. G., and Froment, G. F., *J. Catal.* **59,** 138 (1979).